

PCCP

Accepted Manuscript



This is an *Accepted Manuscript*, which has been through the Royal Society of Chemistry peer review process and has been accepted for publication.

Accepted Manuscripts are published online shortly after acceptance, before technical editing, formatting and proof reading. Using this free service, authors can make their results available to the community, in citable form, before we publish the edited article. We will replace this *Accepted Manuscript* with the edited and formatted *Advance Article* as soon as it is available.

You can find more information about *Accepted Manuscripts* in the [Information for Authors](#).

Please note that technical editing may introduce minor changes to the text and/or graphics, which may alter content. The journal's standard [Terms & Conditions](#) and the [Ethical guidelines](#) still apply. In no event shall the Royal Society of Chemistry be held responsible for any errors or omissions in this *Accepted Manuscript* or any consequences arising from the use of any information it contains.

Unconventional resistive switching behavior in ferroelectric tunnel junction

Cite this: DOI: 10.1039/x0xx00000x

H. J. Mao,^{ab} C. Song,^{b†} L. R. Xiao,^a S. Gao,^b B. Cui,^b J. J. Peng,^b F. Li^b and F. Pan^{b*}

Received 00th January 2012,
Accepted 00th January 2012

DOI: 10.1039/x0xx00000x

www.rsc.org/

We investigate an unconventional resistive switching (RS) behavior in $\text{La}_{0.67}\text{Sr}_{0.33}\text{MnO}_3/\text{BaTiO}_3/\text{metal}$ (LSMO/BTO) ferroelectric tunnel junctions (FTJs), which is dominated by the variation of barrier potential profile modulated by the migration of oxygen vacancies in the p -LSMO/ n -BTO junction. The LSMO/BTO/Co junction exhibits remarkable self-rectifying effect ascribed to the high-density interface state at the BTO/Co interface, in contrast to the symmetric conductivity when the top metal electrode is inert Pt. The effects of ferroelectric polarization on the RS behavior are also emphasized. Our work builds a bridge between FTJs and resistive random access memories.

Introduction

In recent years, ferroelectric tunnel junction (FTJ), composed of two conductive electrodes sandwiching an ultrathin (<5 nm) ferroelectric barrier, has attracted increasing attention in both fundamental and application research.¹ It has been listed as one of the most promising memories in international technology roadmap for semiconductors of 2013.² Theoretical^{3,4} and experimental^{5,6} studies suggest that the asymmetry in the potential profile (*i.e.* different barrier height) for opposite polarization directions, which is related to the depolarization field induced by the incomplete screening effect of the adjacent electrodes with different screening length on the polarization charges, generates the tunnel electroresistance (TER). The conversion between high-resistance state (HRS) and low-resistance state (LRS) in FTJs is realized by applying pulse voltages close to the coercive field of the ferroelectric barrier on the FTJ devices. This process is quite similar to resistive switching (RS) in resistive random access memory (RRAM).^{7–12} Moreover, during the past years, increasing attention has been attracted to the RS phenomenon in ferroelectric heterostructures, based on BiFeO_3 (Refs.13–15) and BaTiO_3 systems.^{16,17}

In RRAM, modulating the potential profile of the p - n junction provides a possible avenue to get RS.^{18,19} In our case, the existence of p -type $\text{La}_{0.67}\text{Sr}_{0.33}\text{MnO}_3$ (LSMO) bottom electrode and n -type BaTiO_3 (BTO) barrier forms the p - n junction. Thus, the scenario mentioned above is fulfilled, and it is quite natural to expect that the RS behaviors can be observed in FTJs manipulated by the potential profile of the p - n junction. In previous publications on FTJs,^{3–6} ferroelectric polarization is always the main focus and the p - n junction is commonly ignored. In addition, in a recent work,¹⁷ the effect of ferroelectric/electrode interface on tunneling electroresistance has been emphasized and the resistive switching requiring larger voltage is also clarified in FTJs, but the role of the ferroelectric/electrode in resistive switching has remained elusive. The experiments described below investigate the different unconventional RS behavior induced by the variation of potential profile of p - n junction in LSMO/BTO/metal (metal

= Co and Pt) FTJs and demonstrate the effects of ferroelectricity-assisted migration of oxygen vacancies on modifying the RS behavior: memory window and rectification.

Experimental

LSMO (30 nm)/BTO (2.8 nm) bi-layer was epitaxially deposited on (001) single crystal $(\text{LaAlO}_3)_{0.3}(\text{LaSrTaO}_6)_{0.7}$ (LSAT) substrate using pulsed laser deposition (PLD) with the reflection high-energy electron diffraction (RHEED) to monitor the growth rate and the surface condition. The stoichiometric ceramic targets of LSMO and BTO were ablated by a KrF excimer laser with the wavelength of 248 nm. The LSMO layer was first grown on the LSAT substrate at 800 °C in an O_2 pressure of 100 mTorr with the pulse repetition frequency of 5 Hz. Then the BTO film deposition was followed at 890 °C in 4 mTorr O_2 with the frequency of 2 Hz. After cooling down to room temperature, the oxide bi-layer was transferred to the magnetron sputtering chamber to deposit the Co or Pt top electrode.²⁰ The microstructure of the stacks was characterized by high-resolution transmission electron microscopy (HRTEM). The ferroelectricity of the BTO barrier was probed by piezoresponse force microscopy (PFM). The junction devices were fabricated by optical photolithography, ion milling and wet-etching. A schematic of the LSMO/BTO/metal devices and measurement setup are depicted in Fig. 1(a). The electrical properties of the devices were measured by an Agilent B1500A semiconductor parameter analyser in the voltage sweeping model. The capacitance–voltage (C – V) curves were evaluated by an Agilent B1505A in the capacitance sweeping model.

Results and discussion

The high-quality of LSMO/BTO/Co FTJs is confirmed by the HRTEM images, as shown in Fig. 1(b). One can clearly see ~30 nm thick LSMO and ~20 nm Co layer with dark contrast in the low-magnified images (the left panel), and between them the thin BTO layer of ~2.8 nm with brighter contrast can be distinguished. A HRTEM image in the right panel displays the high-quality epitaxial LSMO/BTO oxide bi-layer, which is

critical for FTJs. PFM tests were conducted to confirm the ferroelectricity of the 2.8 nm BTO thin film on un-capped LSMO/BTO bi-layer. Alternative d.c. bias of $-4\text{ V} | 4\text{ V} | -4\text{ V} | 4\text{ V} | -4\text{ V}$ were applied to an area of $1 \times 5\ \mu\text{m}^2$, and then a 50 mV a.c. voltage with the frequency of 80 kHz was utilized to read the phase reversal. Corresponding out-of-plane PFM phase image is presented in Fig. 2(c). Apparent 180° phase contrast implies the occurrence of the ferroelectric switching in the film. Phase and amplitude hysteresis loops presented in Fig. 1(d) also indicate the ferroelectric nature of the ultrathin BTO. The local coercive voltages are approximately $+0.5$ and -1 V, where the shift can be explained by asymmetric electrode with different work functions (WF).²¹

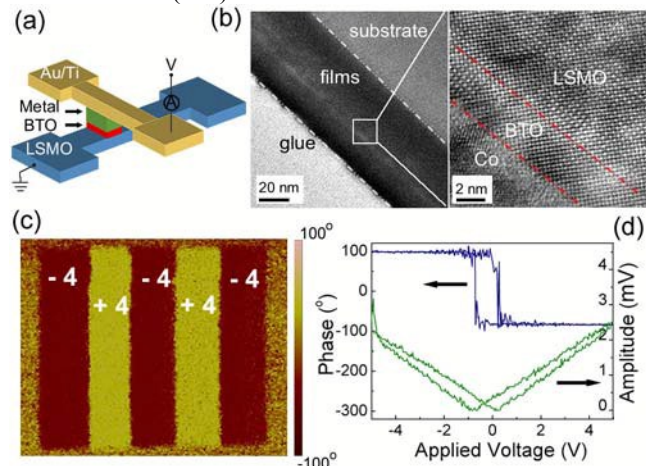


Fig. 1 (a) A schematic of the three-dimensional LSMO/BTO/metal (metal = Co and Pt) device. (b) Cross-sectional low-resolution (left panel) and high-resolution (right panel) TEM images of the LSMO/BTO/Co films. (c) PFM out-of-plane phase image recorded after applying a series of $-4\text{ V} | 4\text{ V} | -4\text{ V} | 4\text{ V} | -4\text{ V}$ voltage with a biased conductive tip. (d) PFM phase and amplitude hysteresis loops at 300 K.

The temperature-dependent current–voltage (I – V) characteristics of the LSMO/BTO/Co junctions are displayed in Fig. 2. During the measurements, the bias voltages were applied on the Co electrode with the LSMO electrode grounded, and neither a forming process nor a current compliance was necessary for activating the memory effect. The most eminent feature observed here is that the set (HRS to LRS) (>10 V) and reset (LRS to HRS) (~ 3 V) voltages, especially the set voltage [Figs. 2(a)], are larger than the room-temperature ferroelectric coercive voltage (~ 1 V) [Fig. 1(d)] obtained by the PFM test on LSMO/BTO bi-layers. This differs dramatically from the tunnel electroresistance generated by the ferroelectric switching when the external voltage is just up to the coercive voltage gained by PFM,^{7–10} which will be discussed later. Figure 2(c) presents the controllable, reversible and reproducible endurance performance of the junctions at 300 K, 200 K, 100 K and 10 K. The gradually enlarged memory windows, defined as $(R_{\text{OFF}} - R_{\text{ON}})/R_{\text{ON}} \approx R_{\text{OFF}}/R_{\text{ON}}$ (OFF/ON), from 100 to 1000 with the decreasing temperature from 300 K to 10 K, are also detected, which is summarized in Fig. 3(a).

A closer inspection of Fig. 2 shows us an asymmetric feature of the I – V curves at positive/negative voltages, especially for LRS. This is the quite characteristic of self-rectifying effect, which has been considered as one of the effective means to solve the notorious sneak-path issue of the RRAM arrays.^{22,23} The rectification ratios calculated at ± 1.5 V for different

temperatures are plotted in Fig. 3(a), reflecting a decrease from 10 to 1.5 with decreasing temperature from 300 K to 10 K. The rectification behavior can be explained by the Schottky barrier at the BTO/metal interface.²⁴ Theoretically, the metal electrode possessing a larger work function associated with higher Schottky barrier would lead to a larger rectification ratio. Control experiments were then performed on FTJs with the same geometry and fabricated in identical lithographic process but with the Co electrode (WF = 5.0 eV) replaced by Pt electrode (WF = 5.7 eV).²⁵ However, the Pt sample exhibits an unexpected symmetrical I – V curve, as shown in Fig. 3(b). Moreover, the rectification phenomena vanish at all the measured temperatures (10–300 K), as summarized in Fig. 3(c). This difference will be discussed below.

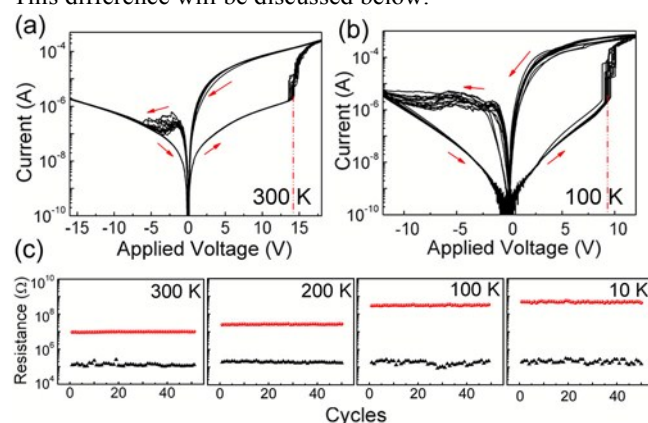


Fig. 2 I – V curves for 10 consecutive switching cycles on the semi-logarithmic scale of a LSMO/BTO/Co device at 300 K (a) and 100 K (b), the red arrows and dashed lines show the sweep direction of the voltage and values of the set voltages, respectively. (c) Corresponding endurance performance between 300 K and 10 K. The resistance was read out at 1 V.

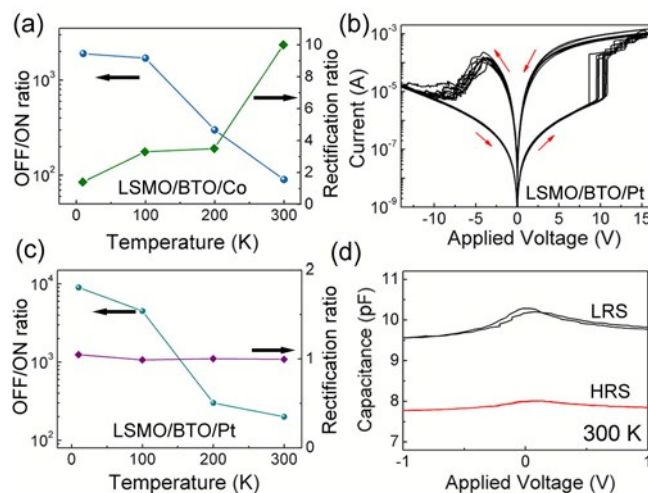


Fig. 3 (a) Temperature-dependent OFF/ON ratio and rectification ratio of LSMO/BTO/Co junctions. (b) I – V curves for 10 consecutive switching cycles on the semi-logarithmic scale of LSMO/BTO/Pt junctions at 300 K. (c) Temperature-dependent OFF/ON ratio and rectification ratio of LSMO/BTO/Pt junctions. Note that the rectification ratio is calculated at 1.5 V. (d) C – V curves of LSMO/BTO/Co junctions at LRS and HRS at 300 K.

Capacitance–voltage measurements can provide information on the state of the potential profile of the barrier, especially the

depletion layer.²⁶ The capacitance in Schottky model is given by $C = \epsilon_0 \epsilon_s S / W_d$, where ϵ_0 is the relative dielectric constant of vacuum, ϵ_s is the dielectric constant of the semiconductor, S is the cell area and W_d is the depletion layer width. As can be seen in Fig. 3(d), the capacitance of the LSMO/BTO/Co FTJs is larger in the LRS (smaller W_d) than that in the HRS, which suggests that the barrier potential profile of LRS is distinct from that of HRS. Similar C - V characteristics of the LSMO/BTO/Pt FTJs are also detected (not shown). The C - V curves confirm that the modulation of the width of depletion layer accounts for the resistive switching.

Based on aforementioned experimental results and analyses, we propose a model considering the barrier potential profile (mainly the depletion layer) of the p - n junction at the interface of LSMO/BTO to interpret the observed RS. As shown in Fig. 4, a depletion layer is created across the p - n junction constructed by p -type LSMO and n -type BTO after reaching dynamic equilibrium due to the interdiffusion of majority carriers.²⁴ When a positive bias voltage is applied on the junctions, the migration of the oxygen vacancies, which is inevitable in complex oxide system,^{16,18,19} is away from the LSMO/BTO interface, resulting in a decrease in the depletion width of the p - n junction, and then the devices are set to LRS.^{27,28}

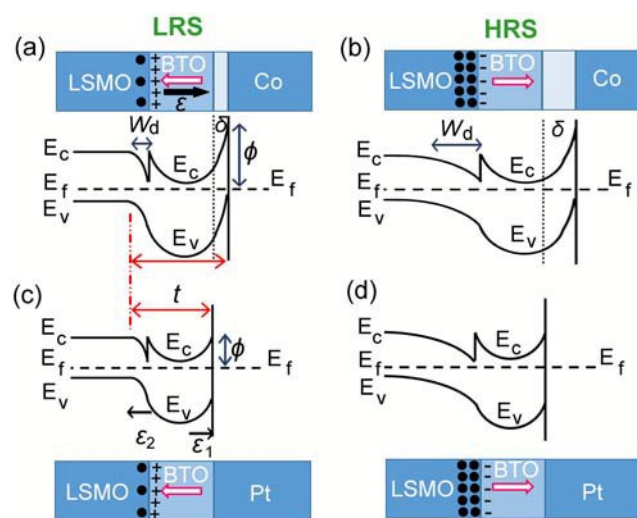


Fig. 4 Schematic diagrams of junction structures and corresponding energy band structure of LSMO/BTO/Co junctions at LRS (a) and HRS (b), as well as of LSMO/BTO/Pt junctions at LRS (c) and HRS (d). In the ferroelectric barriers, the red feint and black solid arrows denote the polarization directions and depolarization field, respectively. The "plus" and "minus" symbols represent positive and negative polarization charges, respectively. The 'dark dot' symbols in the LSMO electrode denote oxygen vacancies. The light blue part between Co and BTO in (a) and (b) represents the interface of oxide layer. ϵ , ϵ_1 (ϵ_2), W_d , t and δ parameter depolarization field, built-in field, depletion layer width, thickness of tunnel barrier layer and thickness of oxide layer, respectively.

As we all know, the migration of the oxygen vacancies is a thermally activated process. Generally, the reduction of the oxygen-vacancy diffusivity in LSMO/BTO bi-layer at low temperatures should lead to an increase of the set voltage.²² However, in our devices the set voltage at 300 K (≈ 14 V) is unusually larger than that at 100 K (≈ 9 V), as shown in Figs.

2(a) and 2(b). When the ferroelectric polarization of BTO is triggered towards LSMO, the positive polarization charges are stimulated at the LSMO/BTO interface [Figs. 4(a) and 4(c)]. Subsequently, the migration of oxygen vacancies to LSMO/BTO interface is hindered by the positive polarization charges via the ferroelectric field effect,²⁹ benefiting for the set process. With decreasing temperature, the ferroelectricity of the BTO is reinforced,⁹ and its influence on the movement of oxygen vacancies becomes much stronger, leading to the anomalous decrease of the set voltage. In contrast, a negative voltage helps the aggregation of the oxygen vacancies towards the interface,³⁰ which increases the depletion width and resets the junctions to HRS. In terms of the enlarged memory windows (Fig. 2), apart from the influence of temperature, the effects of ferroelectricity of BTO also cannot be ignored due to its function of preventing and driving the oxygen vacancies to the LSMO/BTO interface at positive and negative voltage, narrowing and widening the depletion layer, respectively.

Given that the set and reset voltages are much larger than the coercive voltage of the BTO at all tested temperature, we attribute this phenomenon to the depletion layer in the p - n junction, through which a current flowing naturally induces a voltage drop. As what has been confirmed, the depletion layer is wider at HRS than LRS resulting in a more pronounced voltage drop, and then a larger external voltage is needed to set the FTJ from HRS to LRS (>10 V) than from LRS to HRS (~ 3 V), and both of which are larger than the coercive voltage of BTO (~ 1 V). In addition, compared with inert Pt, Co is a relatively active metal, and then a thin oxide layer is formed at the BTO/Co interface, which leads to a voltage drop and makes the switching voltage (especially the set voltage) of Co devices (≈ 14 V) larger than that of Pt devices (≈ 10 V) as shown in Figs. 2(a) and 4(b), respectively. This is similar to the scenario that the voltage needed to reverse the polarization state of ultrathin ferroelectric films is always larger than its intrinsic coercive voltage due to the presence of a non-ferroelectric layer at the film/electrode interface which creates a voltage drop.³¹⁻³³

We now turn towards the distinct self-rectifying behavior for the FTJs with different top electrodes (Co or Pt). For the FTJs with Co electrode, the energy band structures at LRS and HRS are shown in Figs. 4(a) and 4(b), respectively. Co is a getter for oxygen and could attract numerous oxygen ions from BTO, as a result oxygen vacancies are left from BTO adjacent to BTO/Co interface, producing a high density of the interface state.²³ It is well known that when the density of interface state is high, the electronic band in a semiconductor bends at the semiconductor/metal interface, independently of the work function of the metallic electrode.¹⁹ Accordingly, a large degree of the band bending at the BTO/Co interface causes a rectification behavior. Such a behavior would also be modified by the polarization switching of the BTO barrier. As shown in Fig. 4(a), when the polarization points toward LSMO, the depolarization field ϵ created by the polarization charges orients to Co, which hinders the migration of the oxygen ions to BTO/Co interface. This process leads to lower density of interface state,³⁴ cancelling somehow the function of band bending. As the ferroelectricity becomes stronger at low temperatures, the self-rectifying effect is reduced profoundly, *i.e.*, the rectification ratio from 10 to 1.5. In addition, Fig. 2(c) provides evidence whether the ferroelectricity modulates the density of interface state. In our system the BTO barrier is only 2.8 nm and the depletion layer in LSMO layer is also very narrow at LRS, therefore the current should be dominated by tunnelling between LSMO and Co. Generally, the magnitude of

the tunnelling current decreases (*i.e.* the resistance increases) with the decreasing of temperature, while the resistances at LRS in Fig. 2(c) remain almost unchanged at all tested temperatures. Note that the ferroelectric polarization results in a lower density of interface state (narrower oxide layer) and narrower depletion layer in LSMO at low temperature, which leads to a smaller tunnelling barrier layer and the tunnelling current would increase. Thus the balance of the two effects on tunnelling current would make the resistances at LRS stay constant.

The situation turns out to be drastically different when the top electrode is Pt. The work function of Pt is larger than that of n-type BTO (4.2 eV),³⁴ and a Schottky barrier is automatically formed accompanied by the creation of a built-in electric field towards Pt (ϵ_1), whereas the opposite orientation of built-in electric field in the *p-n* junction (ϵ_2) is also formed. When a positive voltage is applied, ϵ_1 is enhanced and ϵ_2 is reduced, while a negative voltage does the opposite. That is, a reverse and a forward diode coexist in the FTJs. If the Schottky barrier at the BTO/Pt interface and the *p-n* junction barrier at LSMO/BTO interface had comparable effects on the conductance of LSMO/BTO/Pt junctions, the rectification behavior cannot be observed. Recalling that the Schottky barrier at the BTO/Co interface and *p-n* junction barrier at LSMO/BTO interface also coexist in the LSMO/BTO/Co junctions, there is distinct self-rectifying effect for this device. We attribute it to the large degree of band bending at the BTO/Co interface, which leads to a higher barrier height ϕ enhancing the ϵ_1 and then the diode at the BTO/Co interface dominates, resulting in the rectification, similar to the case at the Ti(Ag)/(Pr,Ca)MnO₃ interface.²⁸

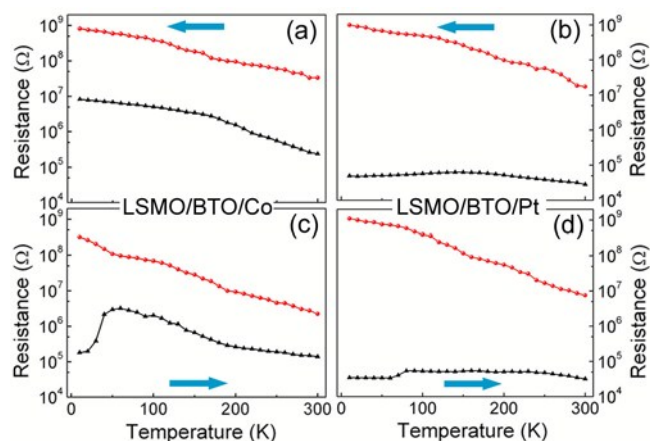


Fig. 5 Temperature-dependent resistance of LSMO/BTO/Co (a) and LSMO/BTO/Pt (b) measured from 300 K to 10 K after “set” to LRS (dark triangle-line) and “reset” to HRS (red circle-line) at 300K. (c) and (d) temperature-dependent resistance of LSMO/BTO/Co (c) and LSMO/BTO/Pt (d) measured from 10 K to 300 K after “set” to LRS (dark triangle-line) and “reset” to HRS (red circle-line) at 10 K. The resistance was read out at 1 V. The blue arrows towards left and right represent the cooling and heating test, respectively.

Temperature-dependent junction resistances ($R-T$) are expected to reaffirm the effect of the barrier potential profile of BTO/metal interface on the RS behavior. Figures 5(a) and 5(b) show the $R-T$ curves of junctions with Co and Pt electrodes during cooling temperature after setting the junctions to LRS or resetting to HRS at 300 K, respectively. It is found that the

HRS resistances increase with decreasing temperature for both junctions, indicating a semiconducting conductance. However, the LRS resistances differ dramatically from each other. The semiconducting conductance remains in the junctions with Co electrode [Fig. 5(a)], which is ascribed to the creation of an additional oxide layer increasing the barrier thickness of Co FTJs [Figs. 4(a) and 4(c)],³⁴ induced by the high density of BTO/Co interface state. Similar oxide layers have been detected at BTO/Fe interface.^{34,35} Differently, the Pt junctions in Fig. 5(b) show a transition from negative dR/dT to positive dR/dT with decreasing temperature. Such a transition was previously observed in magnetic tunnel junctions where the presence of pinholes connecting two ferromagnetic electrodes.^{36–38}

Figures 5(c) and 5(d) respectively present a comparison of the $R-T$ curves of the junctions with Co and Pt electrodes recorded during the heating process from 10 K to 300 K. The resistance at LRS of the Co junction exhibits a cusp at around 50 K and then a downward tendency with further increasing temperature to 300 K. According to the discussion above, the oxide layer at the BTO/Co interface shrinks associated with lower density of interface states because of stronger ferroelectricity at low temperatures,²⁸ the existence of pinholes connecting the two electrodes probably dominates the metallic conductance during 10–50 K. As the temperature increases, the ferroelectricity is weakened and the migration of the oxygen ion becomes active accompanied by the formation of the oxide layer which is much more resistive than Co, leading to the semiconducting conductance, as shown in Fig. 5(c). Apparently, the resistance curves of the Pt sample in Fig. 5(d) show a similar temperature dependence as Fig. 5(b), irrespectively of HRS and LRS states, because the high-density interface states which can be tuned by ferroelectricity do not exist at the BTO/Pt interface with the use of inert Pt. The dependence of *p-n* junction resistance on the temperature is not taken into account, because the LSMO/BTO *p-n* junctions contribute the same to the $R-T$ curves in LSMO/BTO/Co and LSMO/BTO/Pt devices.

Conclusions

In summary, we observe a pronounced RS behavior in LSMO/BTO/metal FTJs ascribed to the modulation of barrier potential profile (mainly depletion layer) of the *p*-LSMO/*n*-BTO junction. The high-density interface state at the BTO/Co interface leads to the apparent self-rectifying effect in the LSMO/BTO/Co junctions. The RS behaviors also affected by the polarization switching of the ferroelectric BTO barrier, which is confirmed by temperature dependent measurements.

Acknowledgements

This work was supported by the National Natural Science Foundation of China (Grant Nos. 51322101, 51202125 and 51231004) and National High Technology Research and Development Program of China (Grant no. 2014AA032901 and 2014AA032904).

Notes and references

^aSchool of Materials Science and Engineering, Central South University, Changsha 410083, China.

^bKey Laboratory of Advanced Materials (MOE), School of Materials Science and Engineering, Tsinghua University, Beijing 100084, China.

†Electronic mail: songcheng@mail.tsinghua.edu.cn

*Electronic mail: panf@mail.tsinghua.edu.cn

- 1 V. Garcia and M. Bibes, *Nat. Commun.*, 2014, **5**, 4289.
- 2 ITRS Roadmap: Emerging Research Devices, The International Technology Roadmap for Semiconductors, <http://www.itrs.net/>, 2013.
- 3 E. Y. Tsybal and H. Kohlstedt, *Science*, 2006, **313**, 181.
- 4 M. Y. Zhuravlev, R. F. Sabirianov, S. S. Jaswal and E. Y. Tsybal, *Phys. Rev. Lett.*, 2005, **94**, 246802.
- 5 M. Gajek, M. Bibes, S. Fusil, K. Bouzehouane, J. Fontcuberta, A. Barthelemy and A. Fert, *Nat. Mater.*, 2007, **6**, 296.
- 6 Z. Wen, C. Li, D. Wu, A. D. Li and N. B. Ming, *Nat. Mater.*, 2013, **12**, 617.
- 7 Q. Liu, J. Sun, H. Lv, S. Long, K. Yin, N. Wan, Y. Li, L. Sun and M. Liu, *Adv. Mater.*, 2012, **24**, 1844.
- 8 X. J. Zhu, W. X. Su, Y. W. Liu, B. L. Hu, L. Pan, W. Lu, J. D. Zhang and R.-W. Li, *Adv. Mater.*, 2012, **24**, 3941.
- 9 C. Schindler, I. Valov and R. Waser, *Phys. Chem. Chem. Phys.*, 2009, **11**, 5974.
- 10 Y. C. Yang, F. Pan, Q. Liu, M. Liu and F. Zeng, *Nano Lett.*, 2009, **9**, 1636.
- 11 R. Waser and M. Aono, *Nat. Mater.*, 2007, **6**, 833.
- 12 F. Pan, S. Gao, C. Chen, C. Song and F. Zeng, *Mater. Sci. Eng. R.*, 2014, **83**, 1.
- 13 J. M. Luo, S. P. Lin, Yue Zheng and B. Wang, *Appl. Phys. Lett.*, 2012, **101**, 062902.
- 14 A. Q. Jiang, C. Wang, K. J. Jin, X. B. Liu, J. F. Scott, C. S. Hwang, T. A. Tang, H. B. Lu and G. Z. Yang, *Adv. Mater.*, 2011, **23**, 1277.
- 15 C. H. Yang, J. Seidel, S. Y. Kim, P. B. Rossen, P. Yu, M. Gajek, Y. H. Chu, L. W. Martin, M. B. Holcomb, Q. He, P. Maksymovych, N. Balke, S. V. Kalinin, A. P. Baddorf, S. R. Basu, M. L. Scullin and R. Ramesh, *Nat. Mater.* 2009, **8**, 485.
- 16 W. J. Ma, S. P. Lin, J. M. Luo, X. Y. Zhang, Ying Wang, Z. X. Li, B. Wang, and Yue Zheng, *Appl. Phys. Lett.*, 2013, **103**, 262903.
- 17 R. Soni, A. Petraru, P. Meuffels, O. Vavra, M. Ziegler, S. K. Kim, D. S. Jeong, N. A. Pertsev and H. Kohlstedt, *Nat. Commun.*, 2014, **5**, 5414.
- 18 S. M. Sadaf, E. M. Bourim, X. J. Liu, S. H. Choudhury, D. W. Kim and H. Hwang, *Appl. Phys. Lett.*, 2012, **100**, 113505.
- 19 Z. Q. Hu, Q. Li, M. Y. Li, Q. W. Wang, Y. D. Zhu, X. L. Liu, X. Z. Zhao, Y. Liu and S. X. Dong, *Appl. Phys. Lett.*, 2013, **102**, 102901.
- 20 H. J. Mao, P. X. Miao, J. Z. Cong, C. Song, B. Cui, J. J. Peng, F. Li, G. Y. Wang, Y. G. Zhao, Y. Sun, L. R. Xiao and F. Pan, *J. Appl. Phys.*, 2014, **116**, 053703.
- 21 C. Song, C. Z. Wang, Y. C. Yang, X. J. Liu, F. Zeng and F. Pan, *Appl. Phys. Lett.*, 2008, **92**, 262901.
- 22 Y. Dong, G. Yu, M. C. McAlpine, W. Lu and C. M. Lieber, *Nano Lett.*, 2008, **8**, 386.
- 23 C. Chen, F. Pan, Z. S. Wang, J. Yang and F. Zeng, *J. Appl. Phys.*, 2012, **111**, 013702.
- 24 S. M. Sze and K. K. Ng, *Physics of Semiconductor Devices* (Wiley-Interscience, Hoboken, 2007).
- 25 H. B. Michaelson, *J. Appl. Phys.*, 1977, **48**, 4729.
- 26 A. Sawa, *Mater. Today*, 2008, **11**, 28.
- 27 P. W. M. Blom, R. M. Wolf, J. F. M. Cillessen and M. P. C. M. Krijn, *Phys. Rev. Lett.*, 1994, **73**, 2107.
- 28 A. Sawa, T. Fujii, M. Kawasaki and Y. Tokura, *Appl. Phys. Lett.*, 2004, **85**, 4073.
- 29 S. Mathews, R. Ramesh, T. Venkatesan, and J. Benedetto, *Science*, 1997, **276**, 238.
- 30 B. Cui, C. Song, G. A. Gehring, F. Li, G. Wang, C. Chen, J. Peng, H. Mao, F. Zeng, and F. Pan, *Adv. Funct. Mater.*, 2015, **25**, 864.
- 31 S. Ducharme, V. M. Fridkin, A. V. Bune, S. P. Palto, L. M. Blinov, N. N. Petukhova and S. G. Yudin, *Phys. Rev. Lett.*, 2000, **84**, 175.
- 32 J. F. M. Cillessen, M. W. J. Prins and R. W. Wolf, *J. Appl. Phys.*, 1997, **81**, 2777.
- 33 N. A. Pertsev, J. Rodriguez Contreras, V. G. Kukhar, B. Hermanns, H. Kohlstedt and R. Waser, *Appl. Phys. Lett.*, 2003, **83**, 3356.
- 34 S. Couet, M. Bisht, M. Trekels, M. Menghini, C. Petermann, M. J. Van Bael, J.-P. Locquet, R. Rüffer, A. Vantomme and K. Temst, *Adv. Funct. Mater.*, 2014, **24**, 71.
- 35 L. Bocher, A. Gloter, A. Crassous, V. Garcia, K. March, A. Zobelli, S. Valencia, S. E-Vedrenne, X. Moya, N. D. Marthur, C. Deranlot, S. Fusil, K. Bouzehouane, M. Bibes, A. Barthélémy, C. Colliex and O. Stéphan, *Nano Lett.*, 2012, **12**, 376.
- 36 S. Mukhopadhyay and I. Das, *Phys. Rev. Lett.*, 2006, **96**, 026601.
- 37 J. Ventura, J. M. Teixeira, J. P. Araujo and J. B. Sousa, *Phys. Rev. B*, 2008, **78**, 024403.
- 38 J. M. Teixeira, J. Ventura, F. Carpinteiro, J. P. Araujo, J. B. Sousa, P. Wisniowski and P. P. Freitas, *J. Appl. Phys.*, 2009, **106**, 073707.